ELSEVIER

Journal of Molecular Catalysis A: Chemical 158 (2000) 67–83

JOURNAL OF MOLECULAR CATALYSIS A: CHEMICAL

www.elsevier.com/locate/molcata

Characterization and catalytic performance of designed surfaces

T. Kawaguchi [1], N. Ichikuni [2], A. Yamaguchi, T. Shido, H. Onishi [3], K. Fukui, Y. Iwasawa [*]

Department of Chemistry, Graduate School of Science, The University of Tokyo, Hongo, Bunkyo-ku, Tokyo 113-0033, Japan

Abstract

This paper attempts to extend our previous studies on the chemical design and characterization of metal atoms/ensembles attached at oxide surfaces and on the in-situ observation of adsorbed molecules on oxide model surfaces. This paper presents a new aspect of catalysis at designed Co/TiO_2, Co/Al_2O_3, Co/SiO_2 surfaces characterized by FT-IR and EXAFS, namely ''Surface catalytic reactions assisted by gas phase molecules'', in which the amount and reactivity of reaction intermediate can be promoted and the structure of reaction intermediate can also be controlled by gas phase molecules undetectable at the surface. This paper also reports the application of one-atomic-layer TiO_2 on SiO_2 as a unique support for an Mo dimer complex to prepare a supported Mo-dimer catalyst. Finally, a new aspect of regulation of a catalytic reaction by monoatomic-height steps on $TiO_2(110)$ relevant to oxide-layer catalysis characterized by STM is also reported.

Keywords: Catalytic reaction mechanisms; Design of active structures; Characterization by EXAFS, FT-IR and STM; Supported Co and Mo catalysts; $TiO_2(110)$ single crystal; NO reduction; Ethanol oxidation; HCOOD dehydrogenation

1. Introduction

Designed surfaces with new and distinct structures, prepared stepwise in a controllable manner by using organic and inorganic metal complexes and clusters as precursors and/or oxide single crystals as model surfaces, provide an opportunity for the development of efficient catalytic molecularly-organized surfaces en route to the ultimate catalyst technologies in the microscopic (atomic/molecular), mesoscopic, and macroscopic (mean-field) regions [1–8]. This class of catalysts and model surfaces can also provide a fundamental implication on the molecular-level mechanism and essential controlling factors for catalysis at surfaces. The longer term challenge to surface chemistry of oxide-supported metal catalysts is to address important issues in activity and selectivity in catalytic reactions, in particular the principles of tuning of metal reactivity and activating reac-

[*] Corresponding author. Fax: +81-3-5800-6892.
E-mail address: iwasawa@chem.s.u-tokyo.ac.jp (Y. Iwasawa).
[1] Present address: Research Center for Characterization and Analytical Science, Kao, 1334 Minato, Wakayama 640-8580, Japan.
[2] Present address: Department of Applied Chemistry, Faculty of Engineering, Chiba University, Yayoi, Inage-ku, Chiba 263-0022, Japan.
[3] Present address: KAST, KSP East-404, Sakado, Takatsu-ku, Kawasaki 213-0012, Japan.

1381-1169/00/$ - see front matter
PII: S1381-1169(00)00043-1

tion intermediates at oxide surfaces. The requirements and design of definite ensemble sizes/structures and reaction fields/environments represent important but as yet few addressed challenge to the field. The role of gas phase molecules in surface catalytic reactions remained to be solved to understand catalytic phenomena at surfaces under reaction conditions [9]. Recently, molecular-level catalyst preparation has become realistic on the basis of modern physical techniques and accumulated knowledge of oxide surfaces, and a clear example of the surface catalytic reaction through strongly adsorbed intermediates assisted by weakly adsorbed molecules present only in the presence of the gas phase molecules has been uncovered on a designed Nb/SiO_2 catalyst [1,10,11].

The use of molecularly-designed catalysts and model surfaces seems to be prerequisite to examining the mechanism and concept of catalysis. There are several approaches to chemical design of active metal sites and ensembles on oxide surfaces by metal–organic and –inorganic complexes and clusters. It has been demonstrated that stable and active structures at catalyst surfaces can be prepared by reaction and strong interaction of inorganic and organic metal-complex precursors with oxides such as SiO_2, Al_2O_3, TiO_2, MgO, La_2O_3, zeolites, etc., as proved by physical techniques [1,2,12]. In the catalysts obtained by this method, metal atoms are attached to oxide surfaces via metal–oxygen bonding at metal–oxide interfaces. The attached metal atoms are often highly dispersed as monomers or distributed forming ensemble structures such as dimers and clusters by the direct bondings to oxide surfaces, depending on the oxidation state of attached metals, the acidity/basicity (intrinsic and impurity-induced) of oxide surfaces, the distribution of hydroxyl groups at oxide surfaces, the nature and behavior of precursors, the loading of attached metals, the preparation methods and conditions, the post treatment conditions, etc. [1–23]. Catalytically-active species may be synthesized at oxide surfaces via attaching a metal complex with appropriate ligands to oxide surfaces, and subsequently chemical transformation of the ligands of the attached complex to reactive ones.

The present study reports the role of gas phase molecules in surface catalytic reactions as a new aspect of catalysis on Co/Al_2O_3, Co/TiO_2 and Co/SiO_2, which are prepared by chemical vapor deposition (CVD) reactions of $Co_2(CO)_8$ on Al_2O_3, TiO_2 and SiO_2, respectively, involving the reaction of surface Co species with surface OH groups as a key step for the catalyst preparation. This paper also reports the preparation of Mo dimers attached on one-atomic-layer TiO_2 on SiO_2 by taking advantage of a selective reaction of $Mo_2(\eta^3-C_3H_5)_4$ with surface OH groups of the TiO_2 layer followed by oxidation with O_2. The catalytic property of the obtained Mo_2/TiO_2 layer$/SiO_2$ sample in ethanol oxidation was examined, and compared to those of Mo_2/SiO_2 and Mo_2/TiO_2. One-atomic-layer oxides have been demonstrated to provide a new class of support for metals and metal oxides and also new catalysis [5,23–27]. The scanning tunneling microscopy (STM) study on $TiO_2(110)$ as a model catalyst also reveals a new suppressive effect of monoatomic-height steps on catalytic formic acid dehydrogenation.

2. Experimental

2.1. Catalyst preparation

2.1.1. Attached Co catalysts

A Co/TiO_2 catalyst was prepared in a similar manner to that for Co/Al_2O_3 and Co/SiO_2 reported in literature [28–30]. $Co_2(CO)_8$ was attached on Al_2O_3 (Degussa Alon C), SiO_2 (Aerosil 200), and TiO_2 (Degussa P25) by a CVD method. Al_2O_3, SiO_2 and TiO_2 were pretreated for 2 h at 573 K before use as supports for $Co_2(CO)_8$. Supporting $Co_2(CO)_8$ on the pretreated Al_2O_3 led to the formation of $Co_4(CO)_{12}$ as shown in Fig. 1. The species with a Co–Co bond distance of 0.254 nm, which is

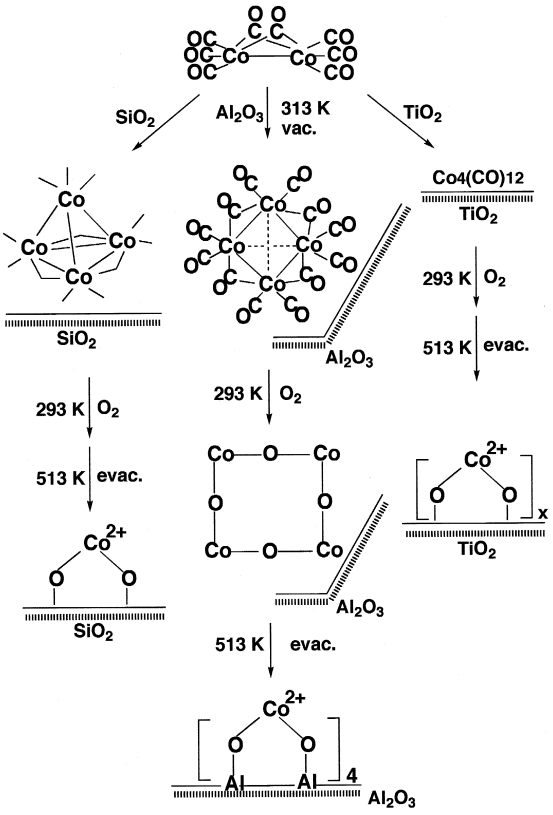

Fig. 1. Preparation steps for the attached Co/Al_2O_3, Co/TiO_2 and Co/SiO_2 catalysts.

larger than 0.249 nm for C_{3v}–$Co_4(CO)_{12}$, was very sensitive to O_2 to be oxidized to a new species $[CoO]_4/Al_2O_3$, accompanied with the disappearance of the direct Co–Co bond and appearance of a new Co–O bond at 0.205 nm, which is shorter than the Co–O bond in CoO crystal (0.2133 nm) [28,29]. When heated at 513 K under vacuum, the $[CoO]_4/Al_2O_3$ reacted with surface OH groups of Al_2O_3, as indicated by the decrease in the intensity of the ν(OH) band centered at 3550 cm^{-1}, to form a $[Co^{2+}]_4/Al_2O_3$ catalyst (denoted as an attached Co/Al_2O_3 catalyst hereinafter) accompanied by the formation of H_2O. The diffuse reflectance UV/VIS spectrum indicates that the Co^{2+} ions are situated in a trigonally distorted T_d position. The bonding scheme is simply illustrated as a bivalent Co^{2+} structure with two Co–O bonds at 0.197 nm, characterized by EXAFS in Fig. 1. The existence of the neighboring Co ions is probed by in-situ EXAFS analysis in the presence of O_2 [31].

The attached Co/SiO_2 catalyst was also prepared in a similar manner [28–30]. However, the EXAFS analysis under any condition revealed no Co–Co bonding, which indicates that Co^{2+} ions are dispersed in an isolated manner at the SiO_2 surface, as monomers rather than an ensemble structure composed of four Co^{2+} ions. The attached Co/TiO_2 catalyst was also prepared in a similar manner to the case of the attached Co/Al_2O_3 catalyst. This catalyst has been not characterized in detail. The Co atoms are suggested to be attached to the TiO_2 surface in a bivalent state with Co–O bond at 0.205 nm [32].

2.1.2. Mo_2/one-atomic-layer TiO_2/SiO_2

The one-atomic-layer TiO_2 on SiO_2 was prepared by using the reaction between Ti(i-$OC_3H_7)_4$ (Soekawa Chemical) and OH groups of the SiO_2 surface (Fuji Davison 952; surface area, 300 m^2/g) according to literature [33]. Ti(i-$OC_3H_7)_4$ vapor was deposited on the SiO_2 surface that was pretreated at 473 K for 2 h in air by a CVD method to react with the OH groups of SiO_2 at 353 K for 2 h. The unreacted Ti(i-$OC_3H_7)_4$ was removed by evacuation at 473 K. After the attaching reaction, the obtained sample was exposed to water vapor at room temperature (RT) to decompose the remaining i-OC_3H_7 ligands, followed by the calcination at 773 K for 2 h. The above procedure was repeated twice to prepare the TiO_2 monolayers on SiO_2.

The Mo attachment on the TiO_2 layer/SiO_2 was performed in a similar manner in the case of Mo_2/SiO_2 [34] and Mo_2/Al_2O_3 [35] by using $Mo_2(\eta^3$-$C_3H_5)_4$. $Mo_2(\eta^3$-$C_3H_5)_4$ was purified by two recrystallization in strictly water-free pentane at 193 K under high purity Ar (99.99995%). The reaction between $Mo_2(\eta^3$-$C_3H_5)_4$ and surface OH groups of the TiO_2 layer/SiO_2 in pentane at 273 K was completed within 20 min. The amount of molybdenum attached on the support was determined from

the initial (before attachment) and the final (after attachment) concentrations of $Mo_2(\eta^3\text{-}C_3H_5)_4$ in pentane by colorimetry [34]. The Mo loading was 1.1 wt.%. The surface allyl-type complexes thus obtained were further evacuated at 350 K for 1 h and converted to Mo^{6+} species by H_2 reduction at 823 K and subsequent O_2 oxidation at 773 K. The preparation steps are shown in Fig. 2.

2.2. Catalytic reactions

Catalytic NO−CO reactions were carried out in a closed circulating system (dead volume: 205 cm^3) equipped with a gas chromatograph (Shimadzu GC-8A) using a 5A Molecular Sieve column and a Unibeads C column in a parallel manner. The reactions of NO alone were also conducted in the same system.

The catalytic ethanol oxidation reactions were also carried out in a closed circulating system

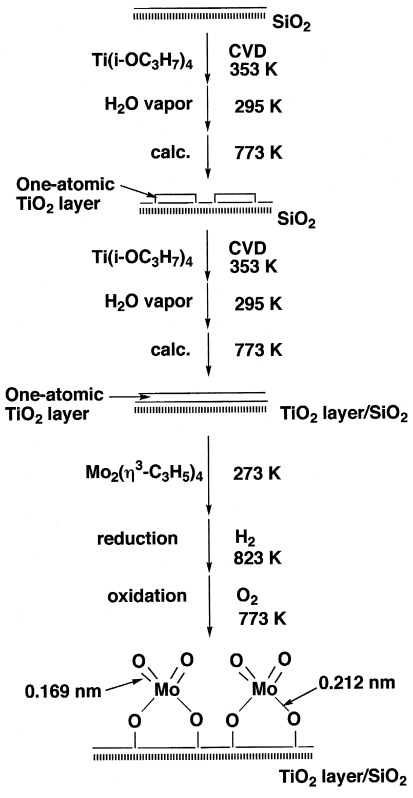

Fig. 2. Preparation steps for the attached Mo_2/TiO_2 layer $/SiO_2$ catalyst.

(dead volume: 170 cm^3) equipped with a gas chromatograph using a Porapak Q column.

2.3. FT-IR measurements

The FT-IR spectra for the NO−CO catalytic system were measured in an IR cell with two CaF_2 windows, which were combined in a closed circulating system, on a JEOL KIR 7000 spectrometer. The spectra were recorded as difference spectra with a 2 cm^{-1} resolution and about 50-s time acquisition by a double-beam method, where the spectra for a sample cell with a catalyst wafer were subtracted by the spectra for the gas phase in a reference cell without catalyst wafer which was also combined in the closed circulating system. FT-IR spectra for the $Mo_2(\eta^3\text{-}C_3H_5)_4$ complex on the TiO_2 layer$/SiO_2$ sample at different temperatures were measured in an IR cell with two NaCl windows which were combined in a closed circulating system, on a JASCO FTIR 7000. The spectra were recorded by a single-beam method, where the difference spectra were taken from the spectra for the Mo_2 complex$/TiO_2$ layer$/SiO_2$ sample and the TiO_2 layer$/SiO_2$ sample.

2.4. XAFS measurements

X-ray absorption fine structure (XAFS) spectra at Mo and Ti K-edges were measured at RT in a transmission mode at the beam lines 10B (for Mo) and 7C (for Ti) of Photon Factory in Institute for Material Structure Science (PF-IMSS) (Proposal No.: 93G060). Synchrotron radiation emitted from a 2.5-GeV storage ring was monochromatized by an Si(311) channel cut monochromator and a Si(111) sagittal focusing double-crystal monochromator, respectively for Mo and Ti XAFS measurements. The sample was transferred to glass cells with two Kapton windows connected to a closed circulating system without contacting air. The detail of the EXAFS analysis has been described in our previous papers [17,33].

2.5. STM observation of TiO_2(110) surfaces

Formic acid (HCOOD) decomposition on a TiO_2(110) single-crystal surface was examined in a UHV-compatible scanning tunneling microscope (JEOL-JSTM4500VT) with an electrochemically etched tungsten tip. Constant current topography was continuously imaged at a rate of 33 s per frame and recorded in video. A polished TiO_2(110) wafer of $6.5 \times 1 \times 0.25$ mm^3 (Earth Chemicals, Japan) gave a sharp (1×1) LEED pattern after repeated cycles of Ar^+ sputtering (3 keV, 0.3 μA) and vacuum annealing at 900 K. Research grade HCOOD gas was purified through trap–thaw cycles [36].

3. Results and discussion

3.1. Surface catalytic NO–CO reactions assisted by gas phase CO molecules

A typical mechanism for heterogeneous catalytic reactions is simply illustrated in Fig. 3(a), where the reaction intermediate (X) is transformed to the product (P) by surface unimolecular decomposition; that is, a stoichiometric reaction step proceeds without aid of other molecules. In contrast to the simple expectation, we have found evidence that the reaction intermediate of an important catalytic reaction can be profoundly influenced by the ambient gas [9]. In the catalytic dehydrogenation reaction of ethanol on the Nb monomer catalyst (Nb/SiO_2),

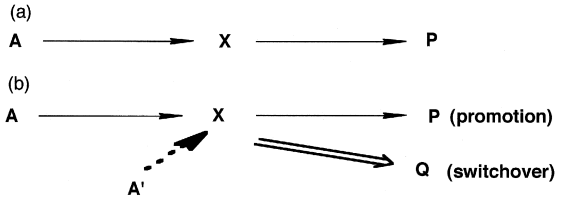

Fig. 3. Surface catalytic reactions assisted by gas-phase molecules; (a) surface catalytic reaction (A → P) via intermediate X; (b) surface catalytic reaction (A → P) promoted by reactant molecule or coexisting molecule A′, where the enhancement of the reaction rate for the formation of P or switchover of the reaction path from P formation is caused by A′.

the Nb-ethoxide intermediate (X) was stable below 600 K and could decompose to a product, ethene ($+H_2O$) (P) only above 600 K. In contrast, in the coexistence of another reactant molecule (A′) the intermediate (X) was activated to decompose to a different product, acetaldehyde ($+H_2$) (Q) even at low temperatures like 473 K. The reaction rate was remarkably promoted and the reaction path was switched over from the dehydration (X → P) to the dehydrogenation (X → Q) assisted by weakly adsorbed molecule A′ [9].

Recently, we have found an example of surface catalytic NO–CO reactions assisted by gas phase CO molecules, which are undetectable at the attached Co catalyst surfaces [2,37]. Slow N_2O formation from NO alone in a closed circulating system was observed above 350 K on the attached Co/Al_2O_3 catalyst. The N_2O formation at 463 K was still slow and the amount of N_2O formed in the first 15 min of reaction was only ca. 2% of total Co quantity dispersed at the catalyst surface. The catalytic reduction of NO in the coexistence of CO to form N_2O and CO_2 by the equation $2NO + CO \rightarrow N_2O + CO_2$, proceeded rapidly compared to the reaction of NO alone. The initial rate of the NO–CO reaction was 23 times larger than that for the NO reaction at 463 K. If CO alone was admitted to the fresh catalyst, no CO_2 was produced, indicating that there existed no reactive oxygen species on the fresh Co/Al_2O_3 catalyst. The activity of the Co/Al_2O_3 catalyst was much higher than that of a conventional impregnation Co/Al_2O_3 catalyst prepared by an impregnation method using an aqueous solution of Co nitrate as shown in Fig. 4. The products of the catalytic NO–CO reaction in the temperature range 353–463 K were N_2O and CO_2. The activation energy was 14 kJ mol^{-1} for the Co/Al_2O_3 catalyst, while it was much larger (46 kJ mol^{-1}) for the impregnation Co/Al_2O_3 catalyst. In the more elevated temperatures N_2O was further converted to N_2, where N_2 and CO_2 were main products by the equations $2NO + CO \rightarrow N_2O + CO_2$ and N_2O

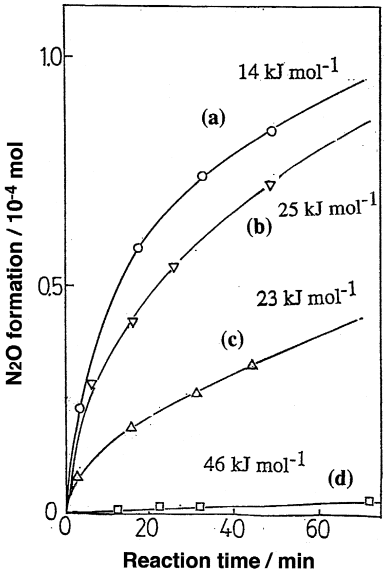

Fig. 4. NO−CO reactions on the attached Co/Al_2O_3 (a), Co/TiO_2 (b), and Co/SiO_2 (c) catalysts and an impregnation Co/Al_2O_3 catalyst (d); NO = 4.0 kPa, CO = 4.0 kPa, reaction temperature = 463 K. The activation energies for the catalysts are also shown.

$+ CO \rightarrow N_2 + CO_2$. In this article, the first reaction step, $2NO + CO \rightarrow N_2O + CO_2$, has been studied from the mechanistic interest. The catalytic activity of the Co/TiO_2 catalyst was a little lower than that of the Co/Al_2O_3 catalyst. The Co/SiO_2 catalyst with an isolated Co^{2+} structure showed a much lower activity than the Co/Al_2O_3 and Co/TiO_2 catalysts as shown in Fig. 4.

The surface catalytic NO−CO reaction on the most active Co/Al_2O_3 catalyst among the examined catalysts was monitored by IR spectroscopy and the gas phase products were analyzed by gas chromatography. Note that CO molecules, which promote the surface NO conversion, were volumetrically and spectroscopically undetectable as adsorbates on the Co/Al_2O_3 catalyst surface [2]. FT-IR spectrum for adsorbed NO molecules in Fig. 5 exhibits two peaks at 1831 and 1776 cm^{-1}, which are assigned to the dinitrosyl (geminal) NO species adsorbed on a Co atom ($Co(NO)_2$) [2]. Besides the dinitrosyl peaks, a small peak at 1821 cm^{-1} is assigned to a linear NO species but the intensity of this peak did not increase in the pressure range 0.25 Pa–4.0 kPa. On the other hand, the reaction rate was of 1.6th order with respect to NO pressure in the same pressure range. Hence, the small linear NO species seems not to contribute to the catalytic NO reduction significantly.

The relative intensity of the symmetric stretching peak at 1831 cm^{-1} and the antisymmetric stretching peak at 1776 cm^{-1} changed with exposure time and also by evacuation. The bond angle (θ) between the two NO ligands on a Co atom (angle: NO−Co−NO) can be calculated by the equation, $I_{as}/I_s = \tan^2(\theta/2)$, where I_{as} and I_s represent the antisymmetric stretching peak intensity (I_{as}) and the symmetric stretching peak intensity, respectively [2,38]. The bond angles (θ) are plotted against exposure time in Fig. 6(a). The amount of adsorbed NO (n_{NO}) is proportional to $I_{as}/\sin^2(\theta/2)$ or $I_s/\cos^2(\theta/2)$, although n_{NO} is not an absolute value for the amount of adsorbed NO. The calculated values of n_{NO} are plotted against time in Fig. 6(b). The change in n_{NO} coincided with the change in the amount of adsorbed NO determined gravimetrically in a separate experiment. Fig. 6(a) and (b) reveals that there are two kinds of dinitrosyls (species A and species B); the dinitrosyl with a

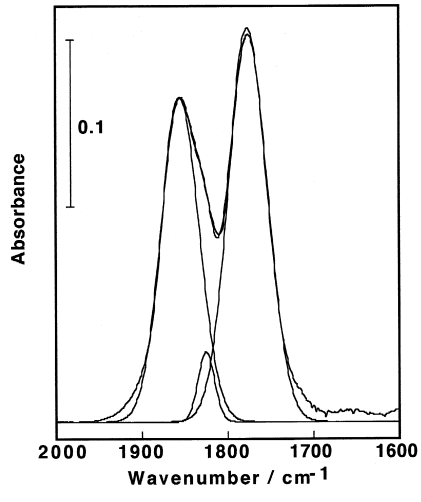

Fig. 5. Peak deconvolution of FT-IR spectrum for NO adsorbed on Co/Al_2O_3; the spectrum at 120 min after NO (4.0 kPa) exposure at 298 K.

small bond angle (species A) is rapidly formed upon NO adsorption and easily desorbed by evacuation at RT, while the dinitrosyl with a large bond angle (species B) is slowly formed and not desorbed by evacuation at RT. We estimated the ratio of species A to species B to be 1:2.1 at RT. From this ratio and the results that the bond angle θ of species B was 107° and the bond angle for a mixture of species A and species B at 120 min of Fig. 6 was 97°, we can estimate the θ for species A at RT to be 80° [2].

Fig. 7 shows the effects of CO on the bond angle and amount of adsorbed NO at 323, 373, 423, 448 and 463 K [2]. The amount of the dinitrosyls decreased with increasing temperature, while the bond angle θ increased with an increase of temperature. When CO was introduced to the system, the bond angle θ of the surface dinitrosyls increased. The degree of the angle expanding was different at temperatures and larger at higher temperatures, and at 323 K, almost zero effect was observed. It was also found that the amount of the dinitrosyls increased by CO admission. Again, the degree of the increase was larger at higher temperatures. Thus, the effects of the ambient CO were large at the temperatures where the catalytic NO–CO reactions proceeded significantly.

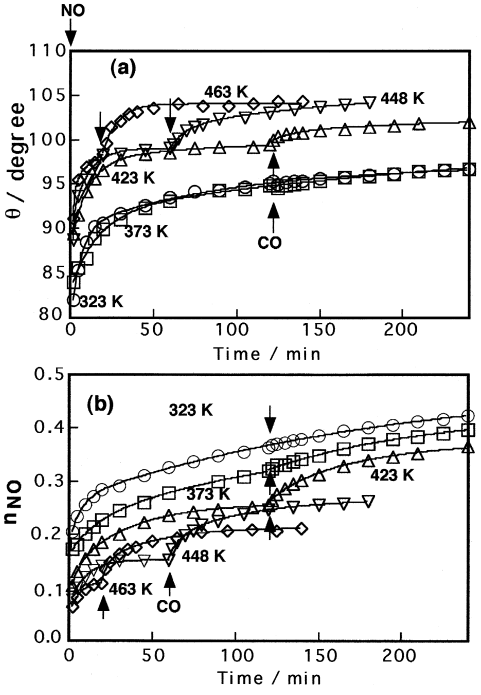

Fig. 7. Time profiles and CO effects of the bond angle and amount of dinitrosyls on Co/Al_2O_3 at 323–463 K; NO = 1.3 kPa, CO = 1.3 kPa.

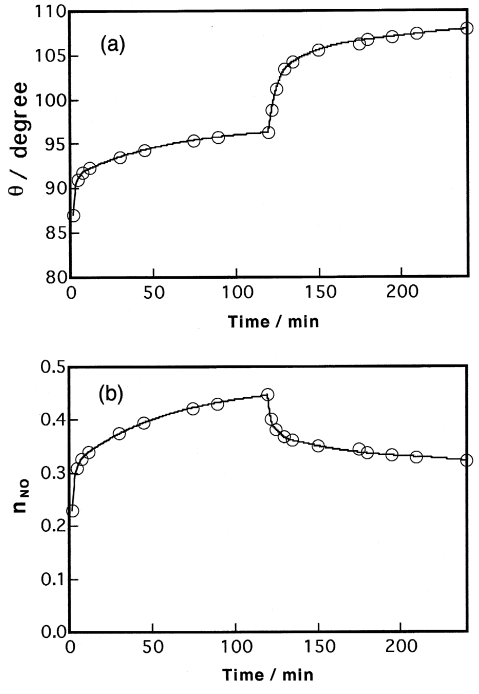

Fig. 6. Time profiles of the bond angle and amount of dinitrosyls on Co/Al_2O_3 at 298 K. The catalyst was exposed to NO of 1.25 kPa at time zero and evacuated at 120 min.

The present finding of the θ extension and the n_{NO} increase promoted by the gas phase CO molecules undetectable at the catalyst surfaces is hardly explained by physical collision of impinging CO molecules. We do not know the exact reason for the observed events at present, but this phenomenon may involve a local structural change of the Co^{2+}–Al_2O_3 interface by CO impinging under the catalytic NO–CO reaction conditions [32].

3.2. Performance of Mo_2/TiO_2 layer / SiO_2 for ethanol oxidation

It may be worthy to briefly summarize the structures of Mo-oxide species supported on

SiO_2 and TiO_2 by different precursors and preparation conditions [3,5,30,39–42].

The interaction of ammonium heptamolybdate often used as a precursor with SiO_2 is generally weak. There is always controversy for the structures of prepared Mo-oxide species in weakly interacting systems presented thus far. The weak interaction resulted in the formation of bulk MoO_3, even for Mo loadings as low as 0.4 wt.% [43], while catalysts with loadings as high as ca.6 wt.% were reported to contain no crystalline MoO_3 [44]. The pH of the impregnating solution or at the silica surface may play a role during the formation of the surface species. At $pH < 2$, heptamolybdate $(Mo_7O_{24})^{6-}$ and octamolybdate $(Mo_8O_{26})^{4-}$ anions are major species, where the SiO_2 surface is charged positively, leading to coulombic interaction to produce polymolybdate species. At $2 < pH < 6$, the heptamolybdate anions species are in equilibrium with monomolybdate anion $(MoO_4)^{2-}$, where the SiO_2 surface is negatively charged, leading to repulsive interaction between the Mo species and the surface, therefore unfavorable for the formation of isolated Mo species at the surface. The low surface pH of SiO_2 itself under ambient conditions also results in the formation of silicomolybdic acid or more likely of trimolybdic clusters $(Mo_3O_{13}^{8-})$ at low Mo loadings on SiO_2. Thus, on SiO_2, pH values high enough for monomolybdate formation are usually not reached; consequently, under hydrated conditions, only polymeric species are detected.

Alkali impurities are known to largely affect the properties of catalysts. It can be assumed that the effects of alkali ions are related to structural changes of the surface compounds or the active centers on the catalyst surface. The structures of alkali-doped Mo/SiO_2 catalysts, e.g. octamolybdate, $Mo_2O_7^{2-}$, and MoO_4^{2-} species, $K_6Mo_7O_{24}$, $Mo_2O_7^{2-}$ dimers, K_2MoO_4, were characterized by a combination of Raman, EXAFS, and X-ray absorption near-edge structure (XANES) [45] and correlated with catalytic performance [46]; impregnation with K_2MoO_4 solutions led to the formation of monomolybdate and $Mo_2O_7^{2-}$ dimers with a low symmetry. Thus, highly polymerized species like MoO_3, octamolybdate, or heptamolybdate are increasingly less favorable relative to monomeric or probably dimeric species.

Instead of aqueous impregnation preparations with ammonium heptamolybdate, preparation procedures via non-aqueous organometallic Mo precursors suppress the formation of crystalline MoO_3, which starts forming even at very low Mo loadings in the impregnation method. Yermakov et al. [8,47] prepared Mo catalysts by taking advantage of reaction of Mo η^3-allyl complex with surface OH groups of SiO_2 and proposed tetrahedrally-coordinated Mo^{6+} ions chemically attached to SiO_2 through two Mo—O—Si bonds. Iwasawa et al. [3,5,17,41] characterized the surface Mo species by many physical techniques such as EXAFS, diffuse reflectance UV/VIS, photoluminescence, etc,. and presented definite structural models such as isolated or paired bidentate MoO_4^{2-} or tetrahedral dimers joined by bridging oxygen, depending on the kind of SiO_2 supports and precursors ($Mo(\eta^3\text{-}C_3H_5)_4$ or $Mo_2(\eta^3\text{-}C_3H_5)_4$), Mo loading, and Na impurity level in the support. Che et al. [48] reported a preparation of catalysts from $MoCl_5$ to possess Mo^{6+} monomeric dispersion. Monodispersed molybdenum oxide was characterized by a high percentage of Mo^{5+} as detected by ESR and by the absence of the intervalence transition ($Mo^{5+} \rightarrow Mo^{6+}$) around l000 nm in the UV/VIS spectra.

Using a non-aqueous preparation method with $Mo_2(\eta^3\text{-}C_3H_5)_4$ and $(\eta^5\text{-}C_5H_5)Mo_2(CO)_4$ as precursors, Roark et al. [49] also concluded from Raman spectra that microcrystalline MoO_3 was not formed on SiO_2 as long as the number of Mo atoms deposited per unit surface remained below the density of silanol groups. High dispersion and high loading of Mo can be reached on SiO_2 via non-aqueous preparation routes.

The XAFS results revealed spreading or break-up of the polymolybdate clusters on SiO_2

upon dehydration. It was proposed from Raman that the polymolybdate cluster (944 cm^{-1}) changed into isolated monooxo sites (986 cm^{-1}) by calcination. However, Desikan et al. [50] observed the 955 cm^{-1} peak, which is assigned to a dioxo structure in a distorted tetrahedral symmetry and not a monooxo structure. Williams et al. [43] concluded from the Raman data that in the dehydrated phase, a structure containing isolated Mo^{6+} ion was formed on SiO_2. In view of the large frequency differences of the Mo=O band found by Williams et al. [43], Desikan et al. [50], and de Boer et al. [51], it is likely that the different surface species were prepared and detected by these groups.

Thus, a variety of structures of Mo species on SiO_2 have been demonstrated depending on precursors, preparation conditions, post-treatments, the atmosphere, Mo loadings, population of surface OH groups, alkali impurity of the support, etc., due to a weak interaction between Mo species and SiO_2 surface.

In contrast to SiO_2 support, TiO_2 support can interact more strongly with Mo species. Ng and Gulari [52] concluded that tetrahedral molybdate species were abundant and coexisting with octahedrally coordinated polymeric molybdates at submonolayer coverages. They concluded that Mo^{6+} ions bind to TiO_2 surface strongly and uniformly until monolayer coverage is reached. Bond et al. [53] demonstrated the presence of Mo monomers at ca. 4 wt.% loadings, which is followed by MoO_3 at higher loadings. They also reported that no highly dispersed monolayer was formed on TiO_2 (anatase).

The structure of the surface Mo-oxide species was described as a highly distorted MoO_6 octahedron by comparing the Mo–O stretching frequency (948–965 cm^{-1}) in the catalyst with that in reference compounds like MoO_4^{2-}, $(NH_4)_2Mo_2O_7$, $K_2Mo_2O_7$, Ba_2CaMoO_6, etc. [54]. Bands at 954 cm^{-1} (assigned to Mo=O stretch) and 875 cm^{-1} (assigned to Mo–O–Mo stretch) indicated the presence of hepta or octamolyubdates, whereas the band at 934 cm^{-1} was observed for a low-loaded sample (1 wt.%), which was interpreted as being due to monomolybdates. The observed frequency is rather high for isolated monomolybdates and alternatively suggests the presence of dimers [55,56]. Raman bands [57] were detected at 993–998 cm^{-1} for Mo/TiO_2 samples irrespective of loading, and together with XANES data, assigned to an isolated, highly distorted tetrahedral monooxo Mo species, but contradicted earlier literature [58–61].

Thus, it seems very hard to prepare a definite molecular structure of Mo-oxide species on SiO_2 and also on TiO_2 by a conventional impregnation method using aqueous media. Instead, at least at low loadings of Mo, we have prepared well-defined Mo structures by using organometallic precursors under controlled and limited conditions and provided a new approach for fundamental research for understanding the origin and mechanism of catalysis [3–5]. In the present study we have prepared a new Mo_2 dimer/TiO_2 layer/SiO_2 catalyst by taking advantage of the reaction of the TiO_2 layer on SiO_2, and found a higher catalytic activity than a Mo_2/SiO_2 catalyst and a higher selectivity for acetaldehyde formation than a Mo_2/TiO_2 catalyst.

We can assume that $Mo_2(\eta^3\text{-}C_3H_5)_4$ with a Mo–Mo bond distance of 0.2183 nm reacts with the TiO_2 layer supported on SiO_2 in a similar manner to that for the Mo_2/SiO_2 catalyst, where $Mo_2(\eta^3\text{-}C_3H_5)_4$ reacted exclusively with surface OH groups of SiO_2. The number of the allyl ligands on an Mo atom in the obtained surface complex was determined by temperature programmed reduction (TPR) up to 823 K under 16.2 kPa of H_2 after evacuation of the surface complex at 353 K for 1 h. The total amount (carbon base) of the desorbed products such as propane, propene, ethane, ethene, etc., was 2.1 C per Mo_2.

Fig. 8 shows the IR spectra for the incipient attached Mo_2 complex on the TiO_2 layer/SiO_2, the sample after evacuation at RT for 10 min, and the sample after evacuation at 353 K for 1 h. There are two peaks at 1627 and 1450 cm^{-1}.

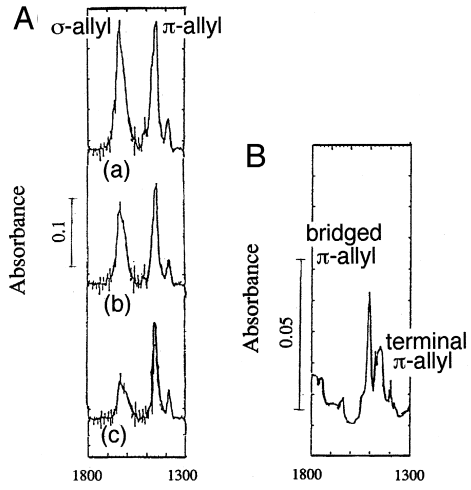

Fig. 8. FT-IR spectra for the Mo_2-allyl complexes attached on the TiO_2 layer/SiO_2 (A) and on KBr (B). (a) The incipient attached Mo_2 complex on TiO_2 layer/SiO_2; (b) evacuation of (a) at room temperature for 10 min; (c) evacuation of (b) at 353 K for 1 h.

The former peak frequency is referred to C=C stretching, and hence, the peak is assigned to the σ-allyl ligand. The latter peak is assigned to π-allyl ligand because the $Mo_2(\eta^3\text{-}C_3H_5)_4$ complex on a KBr disk showed a peak at 1457 and 1510 cm^{-1} for terminal-type π-allyl and bridge-type π-allyl ligands, respectively. The π-allyl ligand on an Rh atom in the attached Rh/TiO_2 catalyst exhibited a peak at 1462 cm^{-1} [39,40]. In consequence, the desorption process of the allyl ligands in the Mo_2 complex/TiO_2 layer/SiO_2 sample is illustrated as follows.

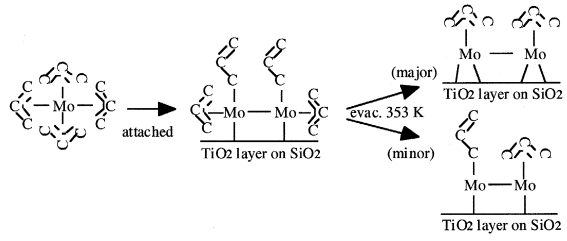

$Mo_2(\eta^3\text{-}C_3H_5)_4$ attached on SiO_2 exhibited the peaks at 1627 and 1503 cm^{-1}, while the complex attached on TiO_2 bulk showed the peaks at 1627 and 1450 cm^{-1}. Thus, the character of the surface Mo_2 complex on the one-atomic TiO_2 layer resembles that of the complex on TiO_2 bulk rather than that of the complex on SiO_2.

The surface Mo-allyl complexes were reduced with H_2 at 823 K, followed by carefully exposing to a small amount of O_2 equivalent to the amount of Mo atoms in the sample at RT, and then they were oxidized to produce hexavalent Mo species with O_2 at 773 K. The obtained Mo^{6+} ions in the Mo_2/TiO_2 layer/SiO_2 were characterized by XANES. The XANES spectrum exhibited a distinct pre-edge peak, as shown in Fig. 9, which indicates that the Mo^{6+} ions are situated in a tetrahedral symmetry.

Fig. 10 shows performance of the attached Mo_2/TiO_2 layer/SiO_2 catalyst for ethanol oxidative-dehydrogenation at 433 K in the absence of O_2. The selectivity determined from the initial rate reached up to more than 99%. The activity for acetaldehyde formation was about twice that of the previous attached Mo_2/SiO_2 catalyst [41]. The formation of acetaldehyde, accompanied with water formation, decreased with reaction time and eventually stopped in the absence of O_2 as shown in Fig. 10. The saturated amount of acetaldehyde produced was half of the amount of Mo atoms loaded on the TiO_2 layer/SiO_2. This stoichiometric feature is similar to that observed on the attached Mo_2/SiO_2

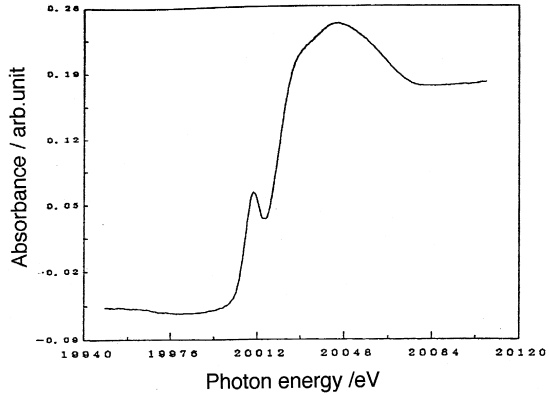

Fig. 9. XANES spectrum for the attached Mo_2/TiO_2 layer/SiO_2 catalyst.

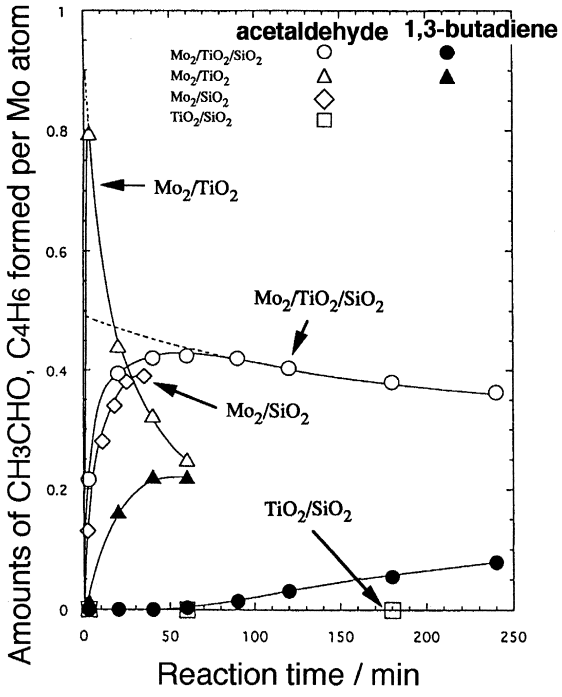

Fig. 10. Reaction profiles for the ethanol dehydrogenation on Mo_2/TiO_2 layer/SiO_2, Mo_2/TiO_2, Mo_2/SiO_2, and TiO_2 layer/SiO_2 catalysts at 433 K in the absence of O_2; cat.: 0.25 g, $P(C_2H_5OH)$: 2.7 kPa.

catalyst, where an Mo dimer unit acted as a reaction site for the conversion of ethanol to acetaldehyde [17,41]. We think that the Mo dimer in the attached Mo_2/TiO_2 layer/SiO_2 catalyst also works as an active unit. The Mo–Mo interaction was observed during the course of the ethanol oxidation by EXAFS as discussed hereinafter. When a Mo_2/TiO_2 catalyst was employed as a catalyst, the amount of acetaldehyde equivalent to the Mo quantity in the Mo_2/TiO_2 catalyst was produced under the identical reaction condition. Hence, on the Mo_2/TiO_2 catalyst, an Mo monomer may be regarded as an active site. From this point of view, the behavior of the Mo_2/TiO_2 layer/SiO_2 catalyst resembles that of the Mo_2/SiO_2 catalyst.

When O_2 was admitted to the reaction system after the saturation of the acetaldehyde formation, the reaction began again. If both ethanol and O_2 were admitted to the system, the ethanol oxidation to produce acetaldehyde proceeded catalytically without stopping. The activation energy for the ethanol oxidation in the presence of O_2 on the attached Mo_2/TiO_2 layer/SiO_2 was 71 kJ mol^{-1}. The activation energy for the ethanol oxidation on Mo_2/SiO_2 was 53 kJ mol^{-1} [41].

To examine the dynamic behavior of the active Mo atoms during ethanol oxidation, we have measured the EXAFS spectra for the Mo_2/TiO_2 layer/SiO_2 catalyst before and after exposing to ethanol at 433 K. Fig. 11(a) shows the Fourier transform of the k^3-weighted EXAFS data for the catalyst before ethanol dehydrogenation in the absence of O_2, which depicts two distinct peaks in the region of 0.1–0.2 nm. These two peaks are straightforwardly assigned to Mo–O judging from the bond distances. This was further confirmed by performing a two-wave curve fitting for the $k^3\chi(k)$ oscillation obtained by the inverse Fourier transform of the region of the two peaks. The best-fit result is listed in Table 1. The Mo=O double bond was observed at 0.169 nm (coordination number (CN): 0.63) and the Mo–O single bond was observed at 0.212 nm (CN: 0.30). These are comparable to 0.170 nm (CN: 0.9) and 0.210 nm (CN: 0.9) though the CN for the Mo_2/TiO_2 layer/SiO_2 catalyst were smaller than those for the Mo_2/SiO_2 [17]. The CNs of the surface bondings determined by EXAFS are often smaller than the real CN expected from the surface structure when the structure is highly distorted. No direct Mo–Mo bonding was found for the fresh Mo_2/TiO_2 layer/SiO_2 catalyst.

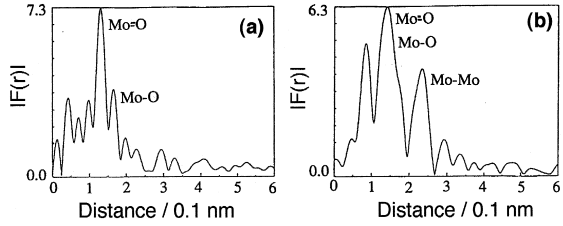

Fig. 11. Mo K-edge EXAFS Fourier transforms for the Mo_2/TiO_2 layer/SiO_2 catalysts before (a) and after (b) exposure to 0.93 kPa of ethanol at 433 K for 7 h in the absence of O_2.

Table 1
EXAFS bet-fit resutls for the Mo_2/TiO_2 layer/SiO_2 catalysts before (A) and after (B) ethanol dehydrogenation at 433 K in the absence of O_2
Reaction condition: $P(C_2H_5OH) = 0.9$ kPa, 7 h, 433 K.
The quality of the parameters determined by EXAFS analysis were estimated by the residual factors.

Sample	Bond	Distance (nm)	CN[a]	ΔE_0 (eV)	DW (10^{-1} nm)[b]
A	Mo−O	0.169	0.6	−0.3	0.034
	Mo−O	0.212	0.3	−15.9	0.032
	Ti−O	0.184	2.9	−9.9	0.060
	Ti−Ti	0.293	0.7	−9.9	0.074
B	Mo−O	0.169	0.8	14.3	0.048
	Mo−O	0.201	1.6	5.1	0.083
	Mo−Mo	0.267	0.3	7.7	0.028
	Ti−O	0.184	2.3	−9.4	0.026
	Ti−Ti	0.298	0.8	−4.6	0.075

[a] Coordination number.
[b] Debye Waller factor.

Fig. 11(b) shows the Fourier transform for the EXAFS data of the catalyst after exposing to 0.93 kPa of ethanol at 433 K for 7 h. A peak assigned for Mo=O bond was observed together with a shoulder assigned for Mo−O bond in the region of 0.1–0.2 nm. Besides Mo−O bonds, a new peak around 0.23 nm (phase shift uncorrected) appeared. This may be assigned to Mo−Mo bond formed by reduction of the Mo^{6+} state to a lower valent state. In fact, when the catalyst was exposed to ethanol at 433 K, acetaldehyde and water were produced, indicating the reduction of the Mo^{6+} ions. The result of Fig. 10 expects the transformation of Mo^{6+} structure to Mo^{5+} structure because of two-electron reduction per an Mo dimer. The detailed analysis of the EXAFS data by three-wave (Mo−O, Mo−O and Mo−Mo) fitting over the region including all the three peaks was performed. The best-fit result is shown in Table 1. The bond distances were determined to be 0.169 (CN: 0.8), 0.201 (CN: 1.6) and 0.267 nm (CN: 0.3) for Mo=O, Mo−O and Mo−Mo, respectively. Since the Mo−Mo bond of the fresh catalyst was not observed at Rt, the appearance of a Mo−Mo bond in the EXAFS result of the catalyst exposed to ethanol at 433 K suggests that the Mo−Mo bond was fixed at a definite distance probably by a bridging oxygen. The bond distances are similar to those for the Mo_2/SiO_2 catalyst after exposing to ethanol at 433 K; 0.171 nm (CN:1.0), 0.194 nm (CN: 1.7) and 0.261 nm (CN: 0.5) for Mo=O, Mo−O and Mo−Mo, respectively. The Mo_2 species (Fig. 11(b)) was oxidized to the original Mo_2 species (Fig. 11(a)) again by oxidation with O_2 at 773 K. In the Mo_2/SiO_2 system, the catalytic ethanol oxidation has been demonstrated to proceed in conjunction with the reversible structural oscillation of the active sites, lateral change by ca. 0.04 nm and vertical change by ca. 0.01 nm. Similarly, the Mo−O bonds markedly changed from 0.212 nm to 0.201 nm and the Mo−Mo bonding feature remarkably changed from no bonding state to a strong bonding state with Mo−Mo bond at 0.267 nm in the course of the dehydrogenation of ethanol. Consequently, the catalytic ethanol oxidation on the Mo_2/TiO_2 layer/SiO_2 catalyst proceeds in conjunction with breaking and formation of Mo−Mo bond as follows.

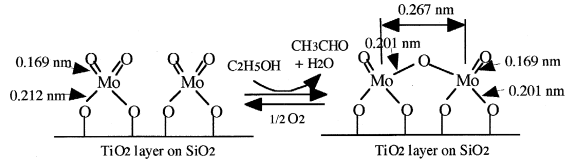

This structural change may be associated with the structure change at the interface. To examine the structural change of the TiO_2 layer, we have performed the EXAFS analysis at Ti K-edge. Fig. 12 shows the Fourier transform of the Ti K-edge EXAFS data for the Mo_2/TiO_2 layer/SiO_2 catalyst before (a) and after (b) exposing to ethanol at 433 K. However, both Fourier transforms were similar to each other. The EXAFS analysis by a curve-fitting technique is shown in Table 1. The Ti−O and Ti−Ti bond distances for the fresh catalyst were determined to be 0.184 and 0.293 nm, respectively, while those for the ethanol-exposed cata-

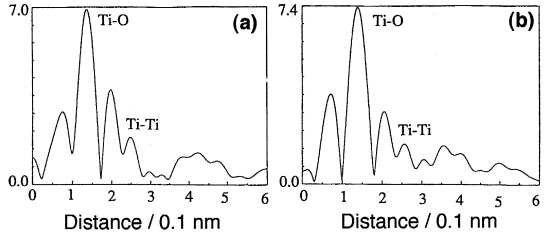

Fig. 12. Ti K-edge EXAFS Fourier transforms for the Mo_2/TiO_2 layer/SiO_2 catalysts before (a) and after (b) exposure to 0.93 kPa of ethanol at 433 K for 7 h in the absence of O_2.

lyst were 0.184 and 0.298 nm, respectively. The Ti–Ti bond distance seems to increase by 0.005 nm. However, it would not be valid to discuss on the structural change from this little change in the Ti—Ti bond distance.

In this study, structural change in the outermost surface, that is the one-atomic TiO_2 layer, to which the active Mo atoms are chemically attached, was not observed, but we suppose that the interface structure may change to assist a structural change in supported metal sites during catalytic reactions.

3.3. Long-range depletion effect of steps on TiO_2(110) for catalytic HCOOD dehydrogenation

The great potential of scanning probe microscopy (SPM) to directly observe the surface structures and reactions at a high resolution has been demonstrated on metal oxide surfaces [1,62]. The most promising ability of STM expected in relation to catalysis research is to discriminate and visualize reaction events occurring at different sites on a surface. Recently the site-specific adsorption of pyridine promoted on four-fold coordinated Ti centers at the steps with particular azimuth orientations on TiO_2(110) has been visualized by STM [63].

We have found the long-range suppressive effect of single-atom height steps at a TiO_2(110) surface on the formic acid (HCOOD) dehydrogenation reaction which takes place over terraces far from the steps.

Individual atoms that constitute a sputter-annealed TiO_2(110)-(1 × 1) surface were resolved by STM [64] and atomic force microscopy operated in a frequency modulated non-contact mode (NC-AFM) [65], as shown in Fig. 13. Each Ti atoms with five-fold coordination in the bright rows of 0.65-nm separation with each other parallel to the [001] direction were clearly observed at a regular interval of 0.30 nm by STM. Atomically resolved NC-AFM image reproduced the (1 × 1) unit, 0.65 × 0.30 nm of the alignment of the bridge oxygen atoms. Several dark sites on the bright lines in the NC-AFM image should be vacancies of the bridge oxygen atoms. The periodicity of these images reproduces an ideal surface truncation of rutile TiO_2(110) single crystal.

When the TiO_2(110) surface heated at 450 K was exposed to a formic acid ambient of 1.3×10^{-6} Pa for 10 min, small particles were formed on the terraces as imaged by STM (Fig. 14(a)). The exposed surface was cooled to RT in the

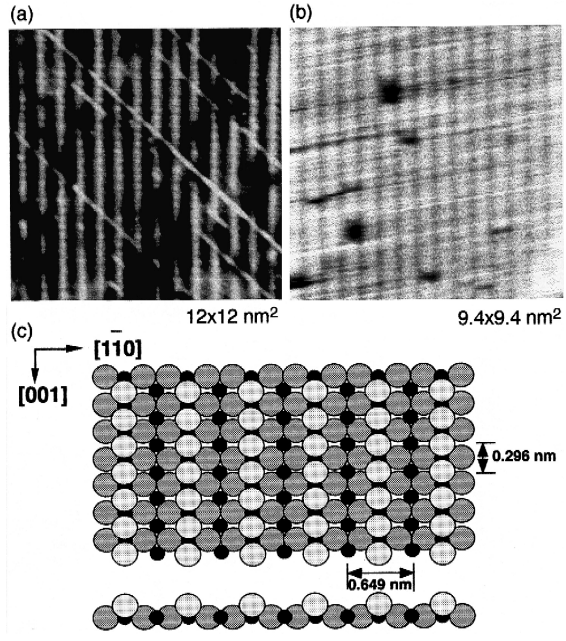

Fig. 13. STM (a) and NC-AFM (b) images and a structure model for a TiO_2(110)-(1×1) surface; STM: $V_s = 1.0$ V, 12×12 nm^2; AFM: $f_o = 270$ kHz, A_o = ca. 30 nm, $\Delta f = 80$ Hz, 9.4×9.4 nm^2.

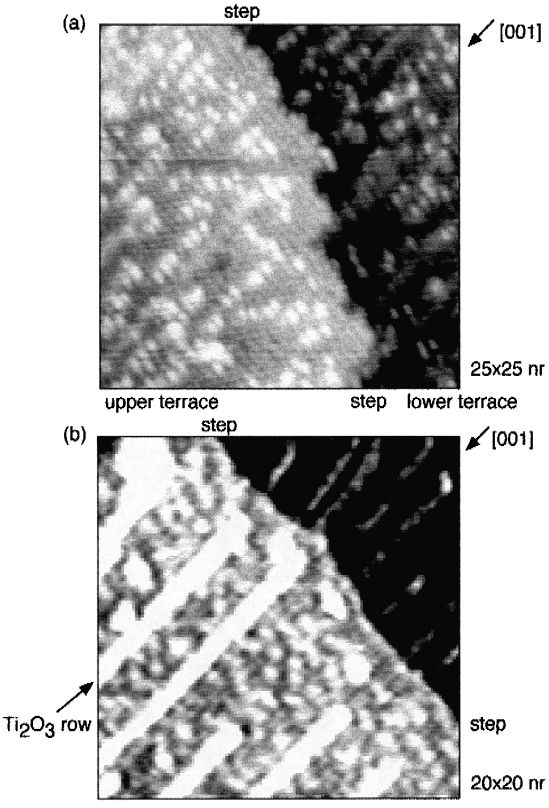

Fig. 14. (a) STM image after the reaction in 1.3×10^{-6} Pa of HCOOD at 450 K for 10 min, followed by evacuation while cooling to room temperature; $V_s = +2.0$ V, $I_t = 0.10$ nA, 25×25 nm^2. (b) STM image during the catalytic reaction of 1.6×10^{-6} Pa of HCOOD at 420 K. The image was recorded at 230 s after exposure to HCOOD at 420 K; $V_s = +1.7$ V, $I_t = 0.20$ nA, 20×20 nm^2.

presence of formic acid vapor and the atmosphere was evacuated to saturate the surface with formate ions in a (2×1) ordered structure. The STM topography was determined at RT. The smallest protrusions presented in a gray scale and arranged in a (2×1) order are the formate ions [66]. Many blips larger and brighter than the formate were observed on the terraces. In the temperature range 420–500 K, the dehydrogenation reaction of formic acid to form H_2 and CO_2 on $TiO_2(110)$ proceeded catalytically and selectively (the activation energy: 15 kJ mol^{-1}) [67]. It was determined from a relative position to the formates on two Ti atoms in a bridge form [66,68–70] that the product particles were located at the on-top position of the bridge oxygen atoms. Thus we assume that a CO_2 molecule adsorbed at the surface on-top site of the bridge oxygen atom forming carbonate (CO_3^{2-}) group makes the product particle. The STM image of the particles in Fig. 14(a) seems elongated, not spherical. The similar elongated feature was observed for carbonate (CO_3^{2-}) produced on an Na-deposited $TiO_2(110)$ surface exposed to CO_2 [71]. The formic acid dehydrogenation on $TiO_2(110)$ takes place by a bimolecular reaction mechanism [67]. Thus, the present observation of CO_3^{2-} provides the following reaction mechanism.

The local number density depended on the distance from the step. Few particles appeared in the proximity of the step, whereas they were produced at random on the terrace far from the step. The near-step area on the terrace looks a depletion belt completely covered with formate ions, as a result.

In-situ STM observation was tried during the particle formation reaction in order to provide the information on location and transport of formate ions as an intermediate of the reaction. A $TiO_2(110)$ surface heated at 420 K was exposed to formic acid vapor of 1.6×10^{-6} Pa in the microscope chamber at $t = 0$. Fig. 14(b) recorded at 420 K shows an image of the exposed surface observed at $t = 230$ s. The number of formate ions imaged as small bright dots increased with exposure time. The number density of formates was often reduced in the proximity of steps. We can assume that the non-uniform distribution of the product particles results from the non-uniform distribution of formate intermediates [36].

These results indicate that the particle formation reaction, which occurred on the terrace far from the step, was suppressed in nanometer-

proximity of single-atom height steps on TiO_2(110). This may be a novel phenomenon. The inverse effect, step-induced enhancement of a reaction, has long been demonstrated [72]. The suppressive effect by single-atom height steps on TiO_2(110) ranges over eight lattice units, 2.4 nm. It is quite important to know how an atom-size surface singularity like the step affects the reactivity of nanometer-proximity. This phenomenon may be a result of diffusion-derived picture. The formate ion may be consumed very fast at the step site by recombinative desorption or decomposition reaction, as is postulated in the step-induced enhancement of reaction. The local number density of the formate ion has to reduce near the step, since adsorption–desorption equilibrium and surface diffusion are coupled to determine the local population of adsorbed species. We have simulated the phenomenon assuming a fast desorption from the step and the boundary condition of $\theta = 0$ at $x = 0$ (θ: particle coverage; x: distance from the step end) and obtained the following equation [36].

$$\lambda_{max} = \sqrt{\frac{D}{k_d}} = \sqrt{\frac{k_h}{2k_d}}\, L_c$$

where λ_{max} is maximum depletion length, and D and k_d represent a diffusion constant and a rate constant for desorption. k_h is a rate constant for hopping migration of formate ions and L_c is the lattice constant of TiO_2(110). When the ratio k_h/k_d is 100, the calculated λ_{max} reproduces the observed depletion-zone length of 2.4 nm.

The present finding may predict that the TiO_2 clusters with < 2.4 nm size show a negligible activity for the catalytic formic acid dehydrogenation, while those with much larger than 2.4 nm size may work as an active catalyst.

4. Summary

(1) The catalytic NO−CO reaction on the attached Co/Al_2O_3 catalyst proceeds through the dinitrosyls as reaction intermediates (X) whose conformation and amount are affected by the gas phase CO molecules. There are no CO molecules at the catalyst surface during the catalytic reactions. The reactivity of the dinitrosyls on the trigonally distorted tetrahedral Co^{2+} ions attached on Al_2O_3 is promoted 23 times by the gas phase CO molecules. In this reaction mechanism, impinging CO molecules (A′) are spectators at the catalyst surface, but they change the conformation and amount of the active species (X), and also behave as reactant. It should be noted that molecules undetectable at surface can give profound effects on the surface structure of reaction sites and promote remarkably the reactivity of surface species. The changes of the amount and conformation of the dinitrosyls by the gas phase CO molecules on the attached Co/TiO_2 catalyst were much smaller and unclear at present. The phenomenon was not observed with the attached Co/SiO_2 catalyst with isolated Co^{2+} ions.

(2) A new attached Mo_2/TiO_2 layer$/SiO_2$ catalyst was prepared by taking advantage of the reaction of $Mo_2(\eta^3\text{-}C_3H_5)_4$ with surface OH groups of the TiO_2 layer followed by successive treatments with H_2 and O_2. The surface Mo structure was characterized by FT-IR, TPR, EXAFS and XANES. The character of the surface Mo_2 complex on the TiO_2 layer resembled that of the Mo_2 complex on TiO_2 bulk. The Mo dimer on the TiO_2 layer$/SiO_2$ worked as active site for ethanol dehydrogenation, whereas on the Mo_2/TiO_2 catalyst the Mo monomer behaved as an active unit. In this sense, the catalytic behavior of the Mo_2/TiO_2 layer$/SiO_2$ catalyst resembled that of the Mo_2/SiO_2 catalyst, but the Mo_2/TiO_2 layer$/SiO_2$ catalyst showed a higher activity than the Mo_2/SiO_2 catalyst for the ethanol dehydrogenation.

(3) We have also found a new kinetic aspect of molecules on terraces and steps on a TiO_2(110)-(1×1) surface by STM, which may be relevant to oxide catalysis. When the TiO_2 surface heated at 400–450 K was exposed to a formic acid ambient of $1\text{–}2 \times 10^{-6}$ Pa, small

particles were formed on terraces. Post-reaction STM observation revealed that the particle formation was strongly suppressed in the vicinity of single-atom height steps. The suppressive effect of step ranged over 2.4 nm into terrace. Formate ions (possible reaction intermediate) were imaged in-situ during formic acid exposure at the reaction temperature. The local density of the formates and hence the product distribution, which were very low near the steps, were simulated by a model. The produced particles were suggested to be carbonates CO_3^{2-} on the bridge oxygen atoms of the $TiO_2(110)$ surface.

Acknowledgements

This work has been supported by Core Research for Evolutional Science and Technology (CREST) of the Japan Science and Technology (JST).

References

[1] Y. Iwasawa, in: Stud. Surf. Sci. Catal., J.W. Hightower, W.N. Delgass, E. Iglesia, A.T. Bell (Eds.), Proc. 11th Int. Congr. Catal., Baltimore Vol. 101 Elsevier, Amsterdam, 1996, p. 21.
[2] A. Yamaguchi, K. Asakura, Y. Iwasawa, J. Mol. Catal. (Special Issue for SHHC, Sounthampton, 1998), 146 (1999) 65.
[3] Y. Iwasawa, Adv. Catal. 35 (1987) 187.
[4] Y. Iwasawa, Catal. Today 18 (1993) 21.
[5] Y. Iwasawa (Ed.), Tailored Metal Catalysts, Reidel, Dortrecht, 1987.
[6] Y. Iwasawa, Elementary reaction steps in heterogeneous catalysis, in: R.W. Joyner, R.A. van Santen (Eds.), NATO ASI, Ser. C Vol. 398 1993, p. 287.
[7] B.C. Gates, L. Guczi, H. Knözinger (Eds.), Metal Cluster in Catalysis, Elsevier, Amsterdam, 1986.
[8] Yu.I. Yermakov, B.N. Kuznetsov, V.A. Zhakarov, Catalysis by Supported Complexes, Elsevier, Amsterdam, 1981.
[9] Y. Iwasawa, Acc. Chem. Res. 30 (1997) 103.
[10] M. Nishimura, K. Asakura, Y. Iwasawa, J. Chem. Soc., Chem. Commun. (1986) 1660.
[11] M. Nishimura, K. Asakura, Y. Iwasawa, in: Proc. 9th Int. Congr. Catal., Calgary Vol. 4 1988, p. 1566.
[12] J.M. Thomas, J. Mol. Catal. A: Chem. 115 (1997) 371.
[13] B. Pugin, F. Spindler, M. Müller, EP 496699-A1 (1991).
[14] B. Pugin, F. Spindler and M. Müller, EP 496700-A1 (1991).
[15] Union Carbide, US Patent 5342907A (1994).
[16] S. Sato, Y. Iwasawa, H. Kuroda, Chem. Lett. (1982) 1101.
[17] Y. Iwasawa, K. Asakura, H. Ishii, H. Kuroda, Z. Phys. Chem. N. F. 144 (1985) 105.
[18] N. Ichikuni, Y. Iwasawa, in: Proc. 10th Int. Congr. Catal., Budapest, 1993, p. 477.
[19] K. Asakura, K.K. Bando, Y. Iwasawa, H. Arakawa, K. Isobe, J. Am. Chem. Soc. 112 (1990) 9096.
[20] K.K. Bando, K. Asakura, H. Arakawa, K. Isobe, Y. Iwasawa, J. Phys. Chem. 100 (1996) 13636.
[21] Y. Izumi, T. Chihara, H. Yamazaki, Y. Iwasawa, J. Phys. Chem. 98 (1994) 594.
[22] Y. Izumi, Y. Iwasawa, Chemtech 24 (1994) 20.
[23] K. Asakura, M. Aoki, Y. Iwasawa, Catal. Lett. 1 (1988) 395.
[24] K. Asakura, Y. Iwasawa, Chem. Lett. (1988) 633.
[25] K. Asakura, Y. Iwasawa, Chem. Lett. (1986) 859.
[26] M. Shirai, K. Asakura, Y. Iwasawa, J. Phys. Chem. 95 (1991) 9999.
[27] Y.-C. Xie, Y.-Q. Tang, Adv. Catal. 37 (1990) 1.
[28] M. Yamada, Y. Iwasawa, Nikkashi (1984) 1042.
[29] Y. Iwasawa, M. Yamada, Y. Sato, H. Kuroda, J. Mol. Catal. 23 (1984) 95.
[30] Y. Iwasawa, Supported catalysts from chemical vapor deposition and related techniques, in: G. Ertl, H. Knözinger, J. Weitkamp (Eds.), Handbook of Heterogeneous Catalysis Vol. 2 Wiley-VCH, 1997, p. 853.
[31] K. Asakura, Y. Iwasawa, J. Phys. Chem. 93 (1989) 4213.
[32] A. Yamaguch, T. Shido, T. Sasaki, K. Asakura, Y. Iwasawa, Proc. 12th Int. Congr. Catal. (2000) to be published.
[33] K. Asakura, J. Inukai, Y. Iwasawa, J. Phys. Chem. 96 (1992) 829.
[34] Y. Iwasawa, M. Yamagishi, J. Catal. 82 (1983) 373.
[35] Y. Iwasawa, Y. Sato, H. Kuroda, J. Catal. 82 (1983) 289.
[36] Y. Iwasawa, H. Onishi, K. Fukui, S. Suzuki, T. Sasaki, Faraday Discus. 114 (1999) in press.
[37] Y. Iwasawa, in: Abstract of 7th Japan–China–USA Symposium on Catalysis, Tokyo, 1995, p. 49.
[38] P.S. Braterman, in: Metal Carbonyl Spectra, Academic Press, 1975, p. 43.
[39] Y. Iwasawa, H. Sato, Chem. Lett. (1985) 507.
[40] Y. Iwasawa, K. Asakura, in: Homogeneous and Heterogeneous Catalysis, VNU Science Press, Utrecht, 1986, p. 75.
[41] Y. Iwasawa, H. Tanaka, in: Proc. 8th Int. Congr. Catal., Berlin, Vol. IV 1984, p. 381.
[42] G. Mestl, T.K.K. Srinivasan, Catal. Rev. 40 (1998) 451.
[43] C.C. Williams, J.G. Ekerdt, J.M. Jehng, F.D. Hardcastle, A.M. Turek, I.E. Wachs, J. Phys. Chem. 95 (1991) 8781.
[44] Y. Barbeaux, A.R. Elamrani, E. Payen, L. Gengembre, J.P. Bonnelle, B. Grzybowska, Appl. Catal. 44 (1988) 117.
[45] N.F.D. Verbruggen, L.M.J. Von Hippel, G. Mestl, B. Lengeler, H. Knözinger, Langmuir 10 (1994) 3073.
[46] N.F.D. Verbruggen, H. Knözinger, Langmuir 10 (1994) 3148.
[47] Y.I. Yermakov, Catal. Rev. — Sci. Eng. 13 (1976) 77.
[48] M. Che, C. Louis, J.M. Tatibouët, Polyhedron 5 (1986) 123.
[49] R.D. Roark, S.D. Kohler, J.G. Ekerdt, D.S. Kim, I.E. Wachs, Catal. Lett. 16 (1992) 77.
[50] A.N. Desikan, L. Huang, S.T. Oyama, J. Phys. Chem. 95 (1991) 10050.

[51] M. de Boer, A.J. van Dillen, D.C. Koningsberger, J.W. Geus, M.A. Vuurman, I.E. Wachs, Catal. Lett. 11 (1990) 227.
[52] K.Y.S. Ng, E. Gulari, J. Catal. 92 (1985) 340.
[53] G.C. Bond, S. Flamerz, L. van Wijk, Catal. Today 1 (1987) 229.
[54] D.S. Kim, Y. Kurusu, I.E. Wachs, F.D. Hardcastle, K. Segawa, J. Catal. 120 (1989) 325.
[55] A.W. Armour, M.G.B. Dreu, P.C.H. Mitchell, J. Chem. Soc., Dalton Trans. 1975 (1975) 1493.
[56] H.J. von Becher, Z. Anorg. Allg. Chem. 474 (1981) 63.
[57] H. Hu, I.E. Wachs, S.R. Bare, J. Phys. Chem. 99 (1995) 10897.
[58] T. Machej, J. Haber, A.M. Turek, I.E. Wachs, Appl. Catal. 70 (1991) 115.
[59] F.D. Hardcastle, I.E. Wachs, J. Raman Spectrosc. 21 (1990) 683.
[60] M.A. Vuurman, I.E. Wachs, J. Phys. Chem. 96 (1992) 5008.
[61] M.A. Bañares, H. Hu, I.E. Wachs, J. Catal. 150 (1994) 407.
[62] Y. Iwasawa, Catal. Surveys. Jpn. 1 (1997) 3.
[63] S. Suzuki, Y. Yamaguchi, H. Onishi, K. Fukui, T. Sasaki, Y. Iwasawa, Catal. Lett. 50 (1998) 117.
[64] H. Onishi, K. Fukui, Y. Iwasawa, Bull. Chem. Soc. Jpn. 68 (1995) 2447.
[65] K. Fukui, H. Onishi, Y. Iwasawa, Phys. Rev. Lett. 79 (1997) 4202.
[66] H. Onishi, Y. Iwasawa, Chem. Phys. Lett. 226 (1994) 111.
[67] H. Onishi, T. Aruga, Y. Iwasawa, J. Catal. 146 (1994) 557.
[68] Q. Guo, I. Cocks, E.M. Williams, J. Chem. Phys. 106 (1997) 2924.
[69] S. Thevuthasan, G.S. Herman, Y.J. Kim, S.A. Chambers, C.H.F. Peden, Z. Wang, R.X. Ynzunza, E.D. Tober, J. Morais, C.S. Fadley, Surf. Sci. 401 (1998) 261.
[70] B.E. Hayden, A. King, M.A. Newton, J. Phys. Chem. B 103 (1999) 203.
[71] H. Onishi, T. Aruga, C. Egawa, Y. Iwasawa, J. Chem. Soc., Faraday Trans. I 85 (1989) 2597.
[72] G.A. Somorjai, Introduction to Surface Science and Catalysis, Wiley, New York, 1994.